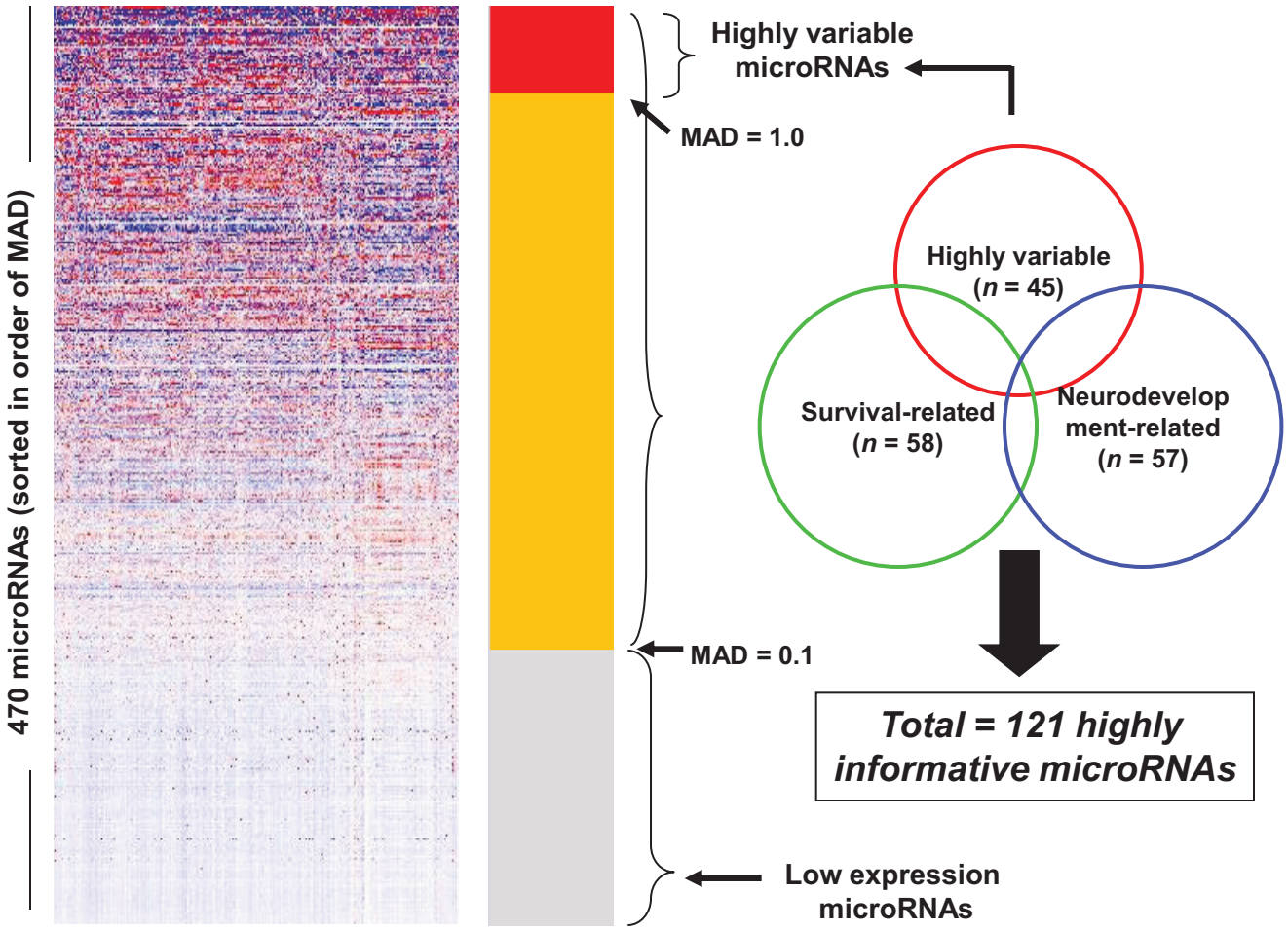

Figure S1. Selection of highly informative microRNAs for glioblastoma clustering analysis. The expression profiles of 470 microRNAs in 261 glioblastoma samples were obtained and normalized as described in Materials and Methods. We filtered microRNAs whose expression level did not change substantially (median absolute deviation or MAD < 0.1). We next selected the microRNAs with highly variable expression (MAD > 1.0), survival-related microRNAs (univariate Cox model, $P < 0.1$) and microRNAs identified from literature review as previously associated with neural development. This yielded 121 highly informative microRNAs for further analysis.

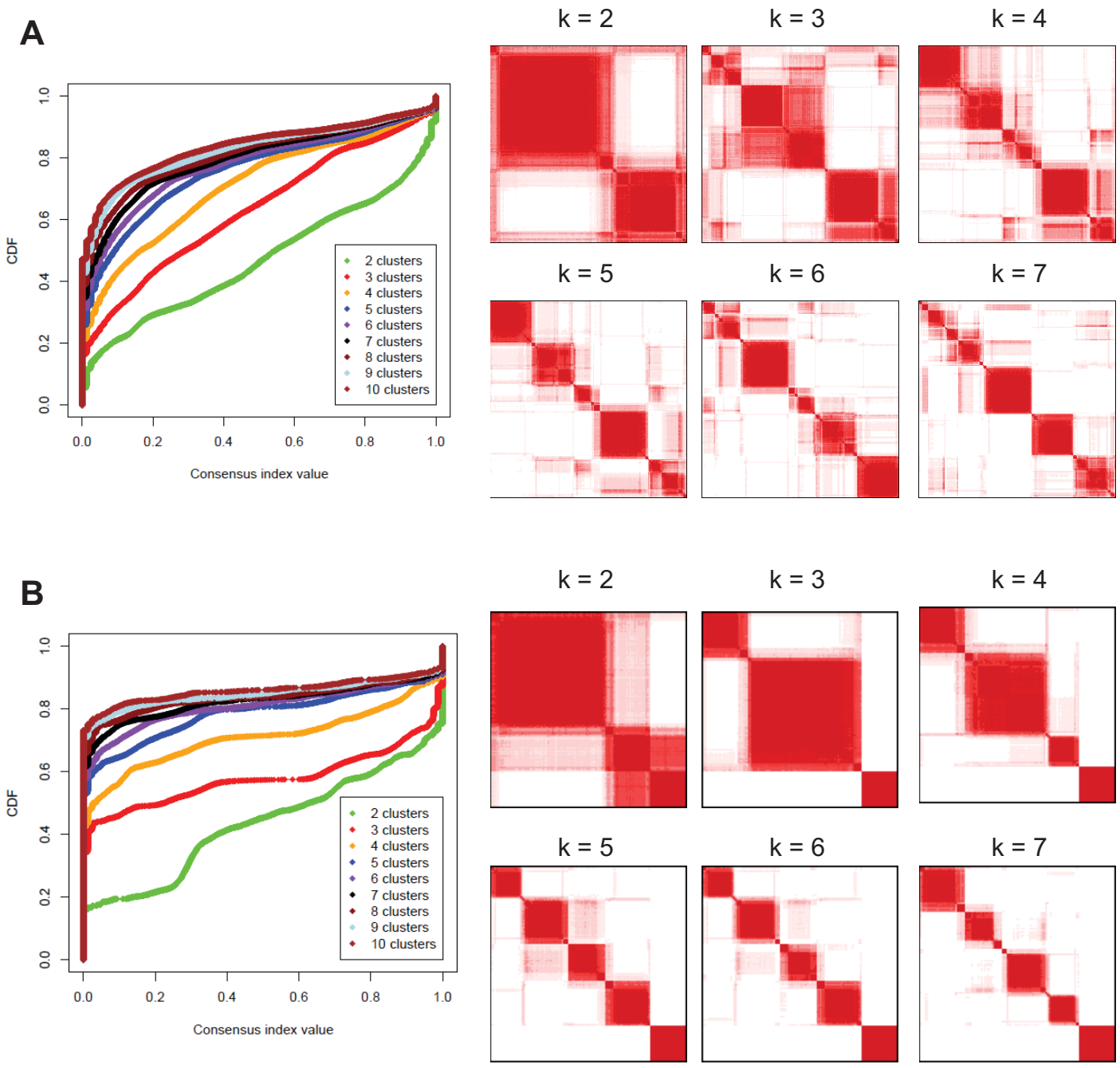

FigureS2. Consensus clustering of glioblastoma samples using microRNAs revealed five glioblastoma subclasses and five microRNA clusters. (A) Consensus clustering CDF (cumulative distribution function) of 261 glioblastoma samples for k = 2 to 10 (left) is shown with consensus matrices for k = 2 to 7 (right). **(B)** Consensus clustering CDF and consensus matrices for 121 microRNAs are shown.

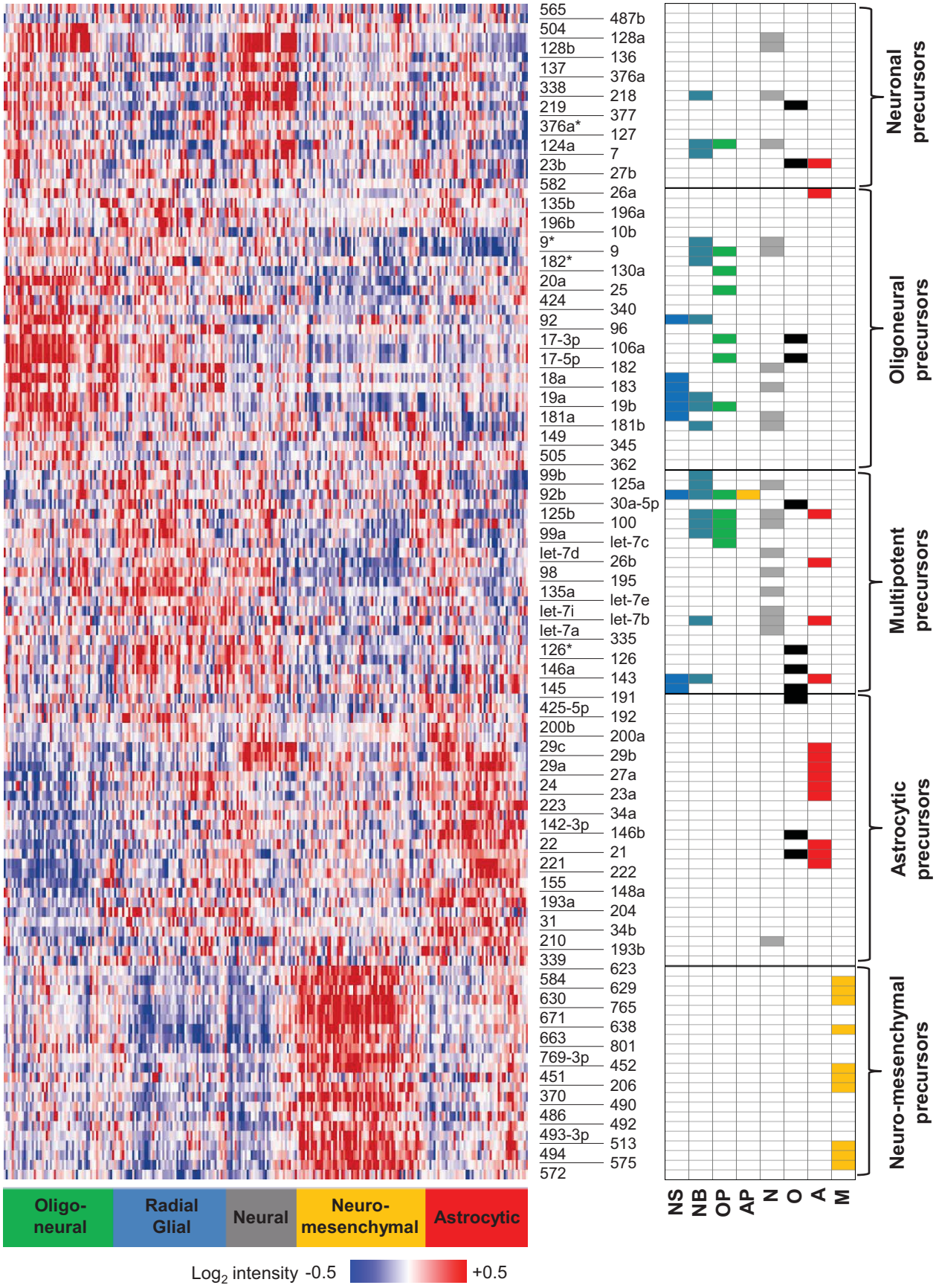

Figure S3. Five microRNA clusters and five glioblastoma subclasses. Consensus clustering of 121 microRNAs in glioblastoma. Neurodevelopmental relationships of selected microRNAs are indicated in the color-coded chart to the right. NS (neural stem cell), NB (neuroblast), OP (oligodendrocyte precursor), AP (astrocyte precursor), N(neuron), O (oligodendrocyte), A (astrocyte), and M (mesenchymal).

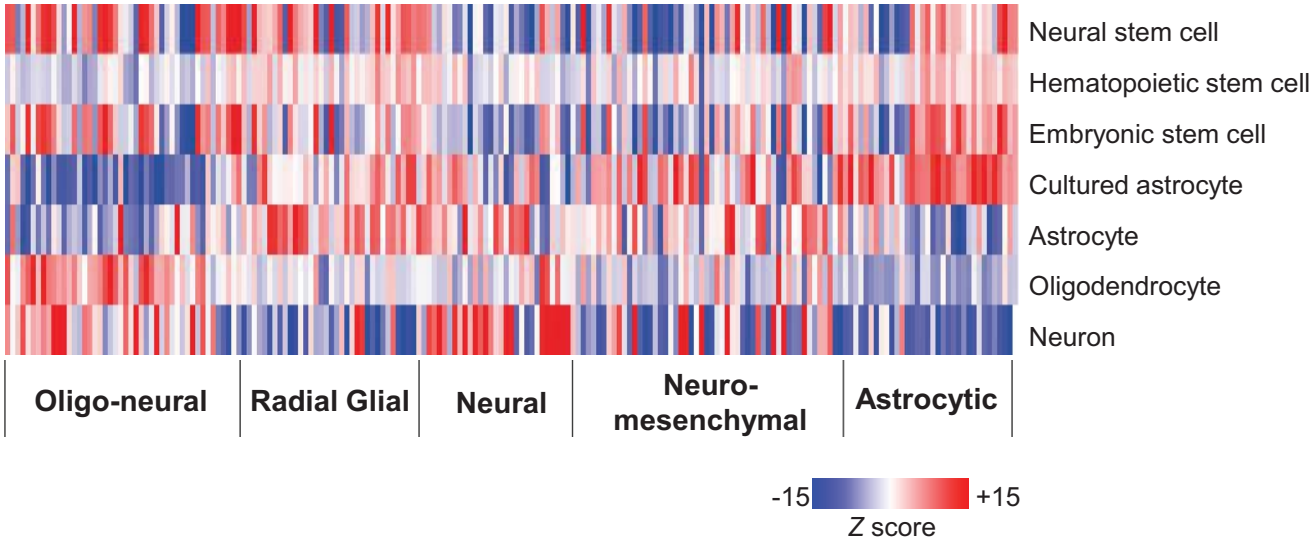

Figure S4. Sample-wise enrichment of mRNA signatures in five microRNA-based glioblastoma subclasses. Gene sets representing up-regulated genes in stem cells (neural, hematopoietic and embryonic stem cells) and differentiated neural cell types (astrocytes, cultured astrocytes, oligodendrocytes, and neurons) were measured in a sample-wise manner. The expression level of genes belonging to a gene set was converted into a *Z*-score and shown in a heatmap. The microRNA-based glioblastoma classification is shown below. Red and blue indicate up- or down-regulation of mRNA signatures, respectively.

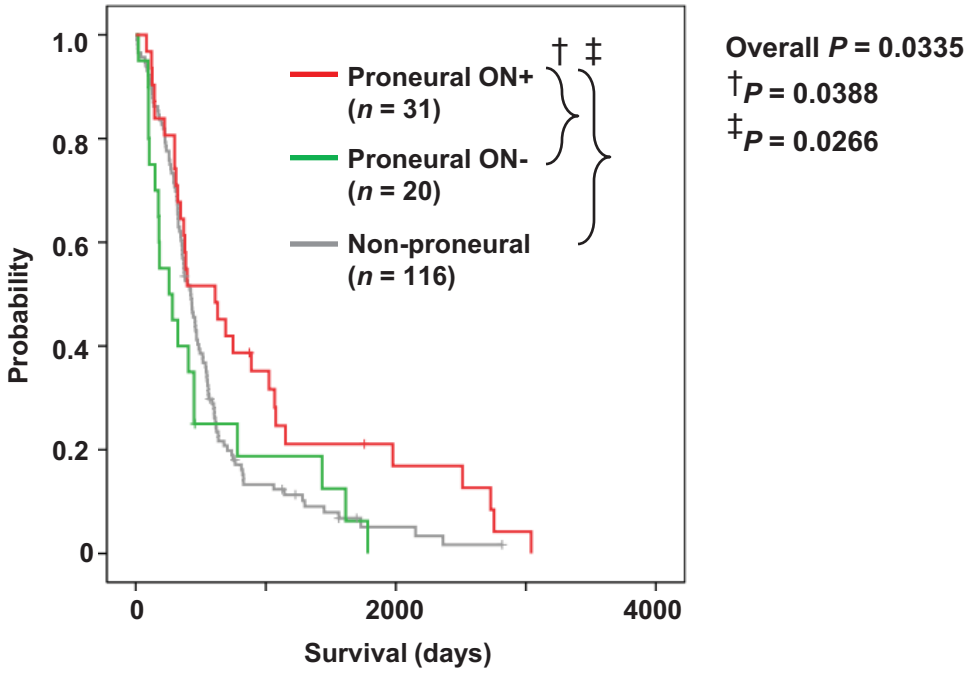

Figure S5. Survival differences among the proneural and non-proneural subclasses. The proneural subclass is separated into those tumors that were also designated as members of the microRNA-based Oligoneural subclass (Proneural ON+; *n* = 31) and those that were not (Proneural ON-; *n* = 20). Kaplan-Meier survival curves are shown to compare the survival difference between these two proneural subclasses and the non-Proneural subclasses (Non-proneural; *n* = 116). Patients with tumors annotated as both Proneural and Oligoneural (Proneural ON+) showed significantly longer survival than those with Proneural ON- tumors and those with Non-proneural tumors.

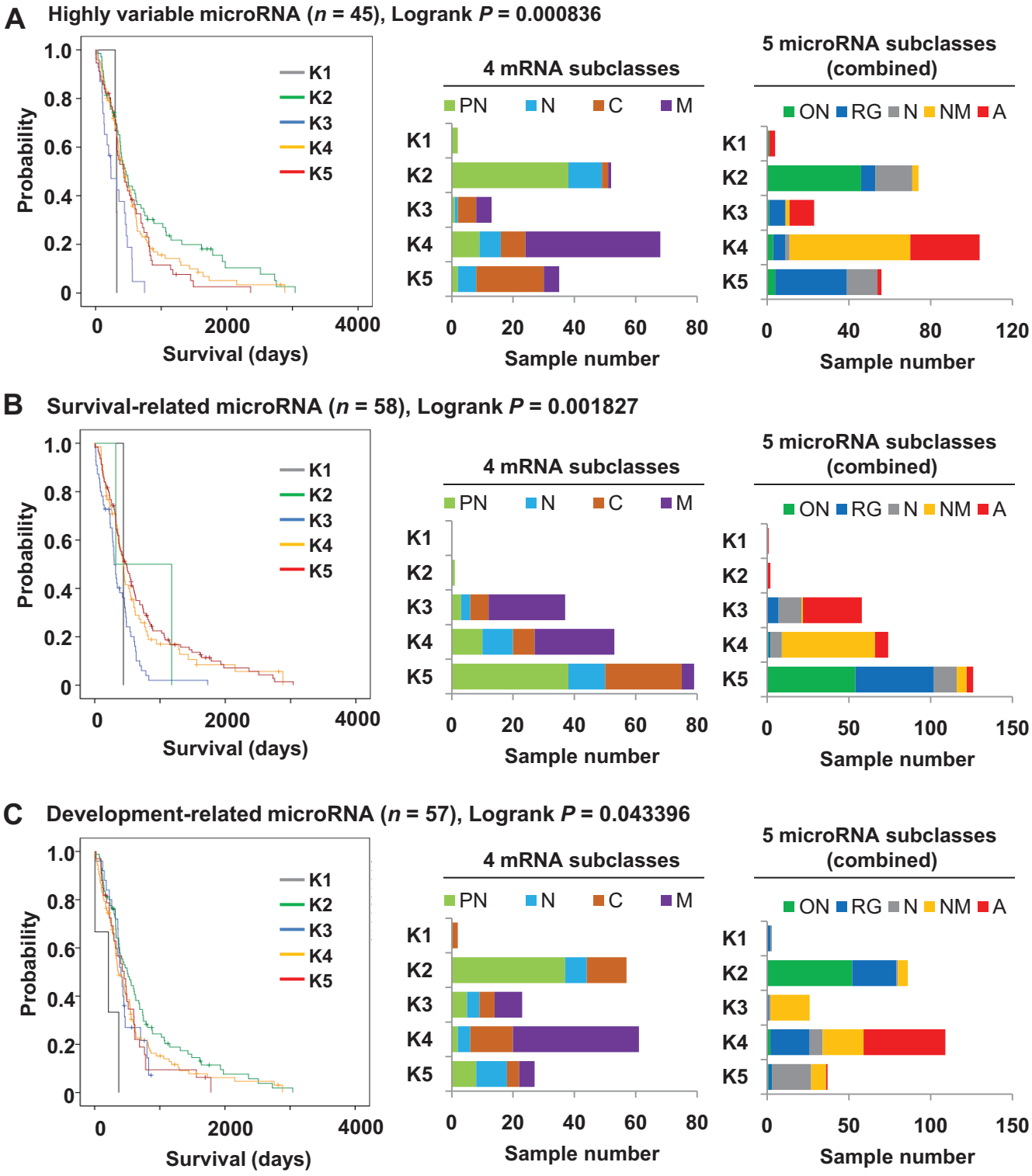

Figure S6. Survival analyses and cross-platform comparisons of glioblastoma clusters defined by microRNA subsets. (A) (*left panel*) Consensus clustering (K = 5) was performed using expression data from a subset of highly variable glioblastoma microRNAs (MAD > 1.0; n = 45). Kaplan-Meier survival analysis shows that the resulting five glioblastoma clusters (annotated as K1 – K5) display a significant difference in survival (P = 0.0008, Logrank). (*middle panel*) Tumor samples in each of the five glioblastoma clusters defined using the highly variable microRNA subset are re-identified using designation derived from the four subclass, mRNA-based classification scheme. (*right panel*) Tumor samples in each of the five glioblastoma clusters defined using the highly variable microRNA subset are re-identified using their designations in the five subclass, 121 microRNA-based classification scheme. **(B)** and **(C)** show results of analyses similar to that shown in **(A)**, except that a survival-related microRNA subset (n = 58) or a neurodevelopment-related microRNA subset (n = 57) was used, respectively. Significant survival differences were observed in all three scenarios. Bar graphs show that several of the subset-generated clusters are enriched for tumors from specific glioblastoma subclasses.

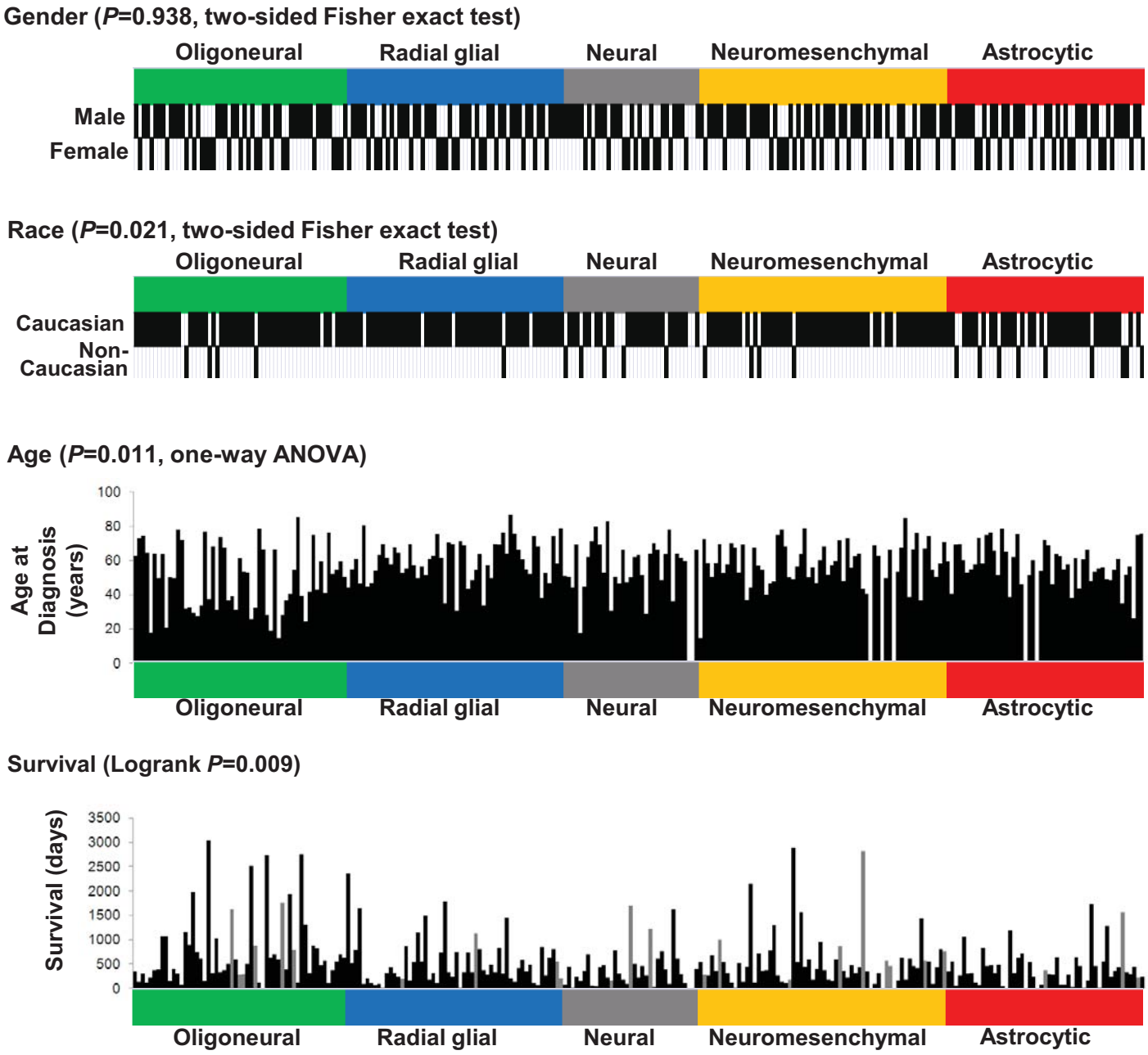

Figure S7. Clinical characteristics of microRNA-based glioblastoma subclasses. For gender and racial analyses, vertical black bars indicate affected individuals. Bar graphs are presented to indicate the age at diagnosis and the survival of individual patients in each subclass. For the survival analysis, grey bars indicate censored data. Statistical tests and *P* values of statistical significance are as indicated.

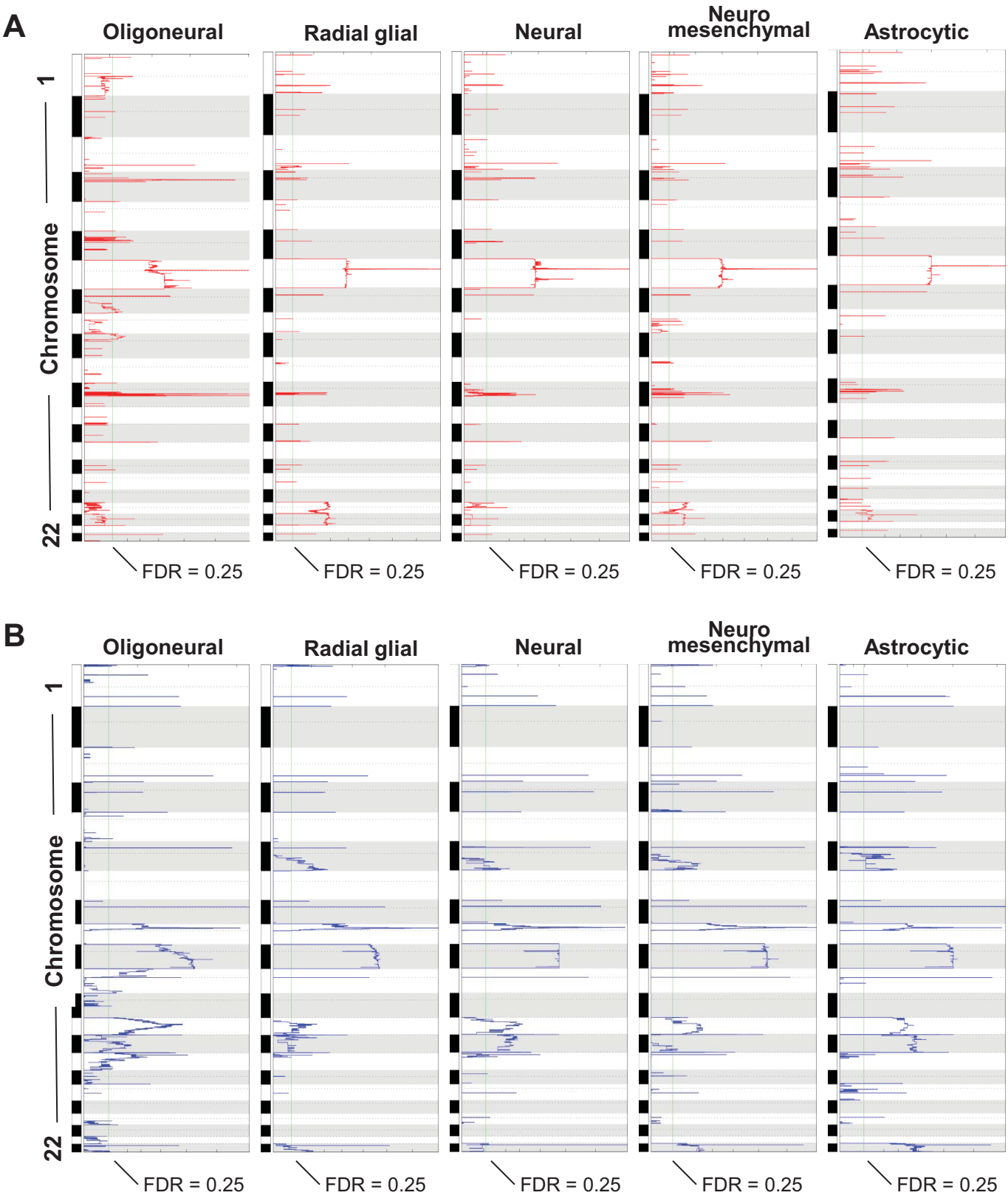

Figure S8. Genome-wide GISTIC analysis of significant copy number alterations in glioblastoma subclasses. (A) For amplifications, the statistical significance (false discovery rate or FDR) for copy number alterations is plotted across the genome for the five glioblastoma subclasses. The threshold FDR of 0.25 for significance is indicated by a green line in each plot. **(B)** For deletions, the FDR for copy number alterations is plotted across the genome for the five glioblastoma subclasses.

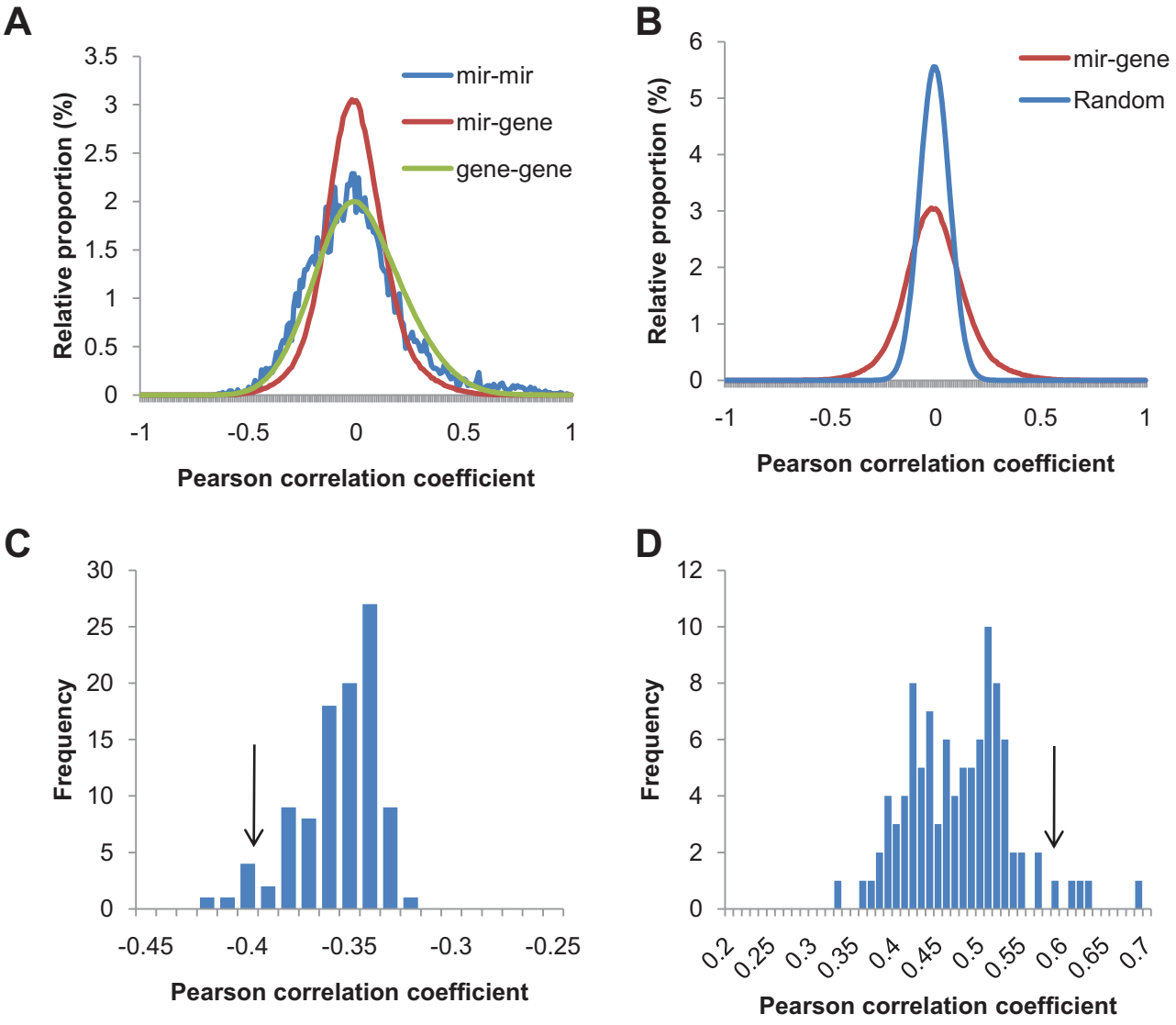

E

	miRanda	PicTar (5way)	PicTar (4way)	TargetScan	Total
Connectivity	159	20	69	83	1116
Total	1283	191	491	629	11861
P value	3.4E-05	0.08364	0.00017	0.00031	

Figure S9. Distribution of correlations between microRNA and mRNA in glioblastoma. **(A)** The distribution of correlations (Pearson correlation coefficients) is shown for three types of pairs; microRNA-vs-microRNA ('mir-mir', blue), microRNA-vs-mRNA ('mir-gene', red) and mRNA-mRNA ('gene-gene', green). The correlation was measured from the expression profiles of 121 microRNAs and 11861 mRNAs in a pairwise manner. **(B)** The microRNA-vs-mRNA correlation was also measured for label-permuted 100 random sets. The distribution of correlations from a random set is shown ('Random', blue) and compared with the actual correlation distribution ('mir-gene', red). **(C)** The distribution of minimum correlation values in 100 permutation sets is shown. The cutoff for a significantly negative correlation was set to be the lower 5th percentile (-0.4; arrow). **(D)** The distribution of maximum correlation values in 100 label-permutation tests is illustrated. The cutoff for a significantly positive correlation was the upper 5th percentile (+0.6; arrow). **(E)** A total of 1116 genes that showed a significant correlation (>+0.6 or <-0.4) with miR-9 were investigated for enrichment with predicted miR-9 target genes. We used three public databases (miRanda, PicTar and TargetScan), from which 159, 20, 69, and 83 miR-9 target genes were curated. Three miR-9 target gene sets were significantly correlated (Fisher's Exact Test $P < 0.05$).

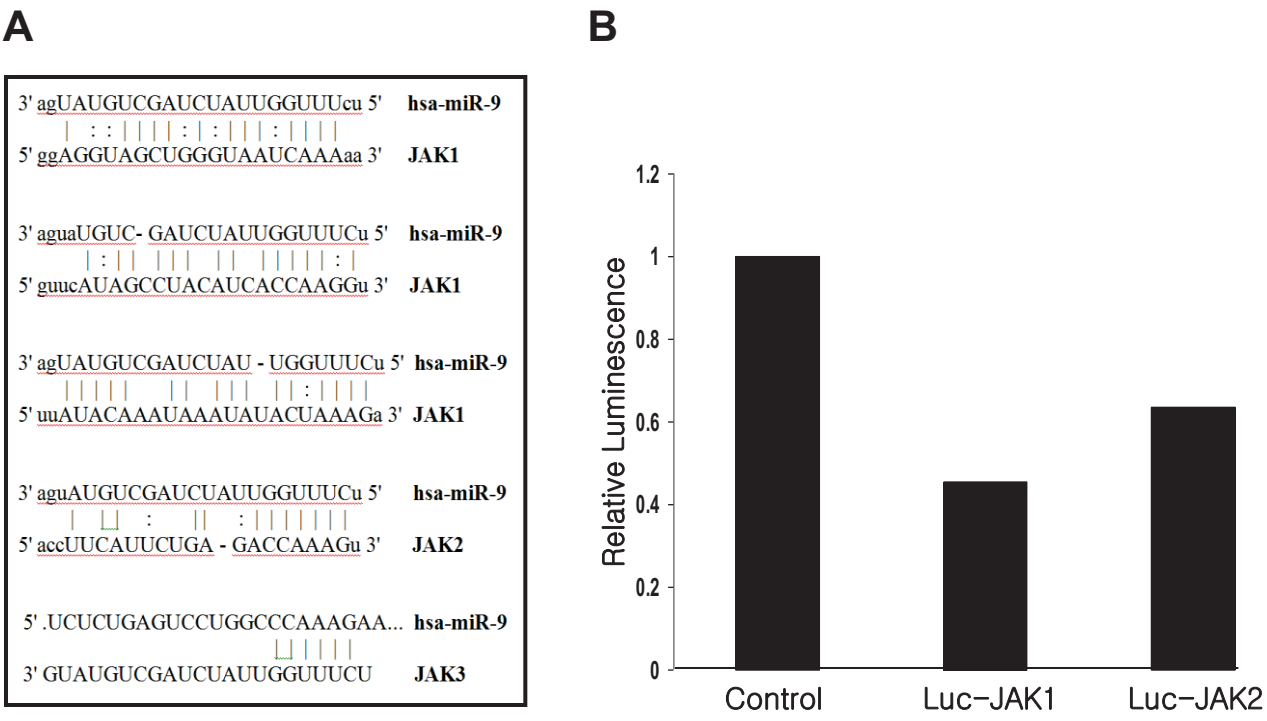

Figure S10. miR-9 directly targets Janus Kinase mRNAs for degradation. (A) Sequence alignment between hsa-miR-9 and 3'UTRs of JAK1. JAK2 and JAK3 mRNAs. Data obtained from www.microrna.org and from www.targetscan.org. **(B)** Luciferase reporter assay in HEK 293 cells. The 3'-UTRs of JAK1 and JAK2 were fused to the C-terminus of firefly luciferase and placed under the control of the CMV promoter. HEK 293 cells were co-transfected with either the JAK1 or JAK2 vector and a β-galactosidase vector to allow for normalization of transfection efficiency. Cells were then exposed to the miR-9 mimic or a scrambled control oligonucleotide (100 μM) for 48 hours. Luciferase activity was detected after administration of luciferin substrate using a luminometer. Data shown are expressed relative to control cells transfected with vectors but exposed to the scrambled oligonucleotide control. The mean of three replicates is shown, and the experiment was repeated in duplicate.

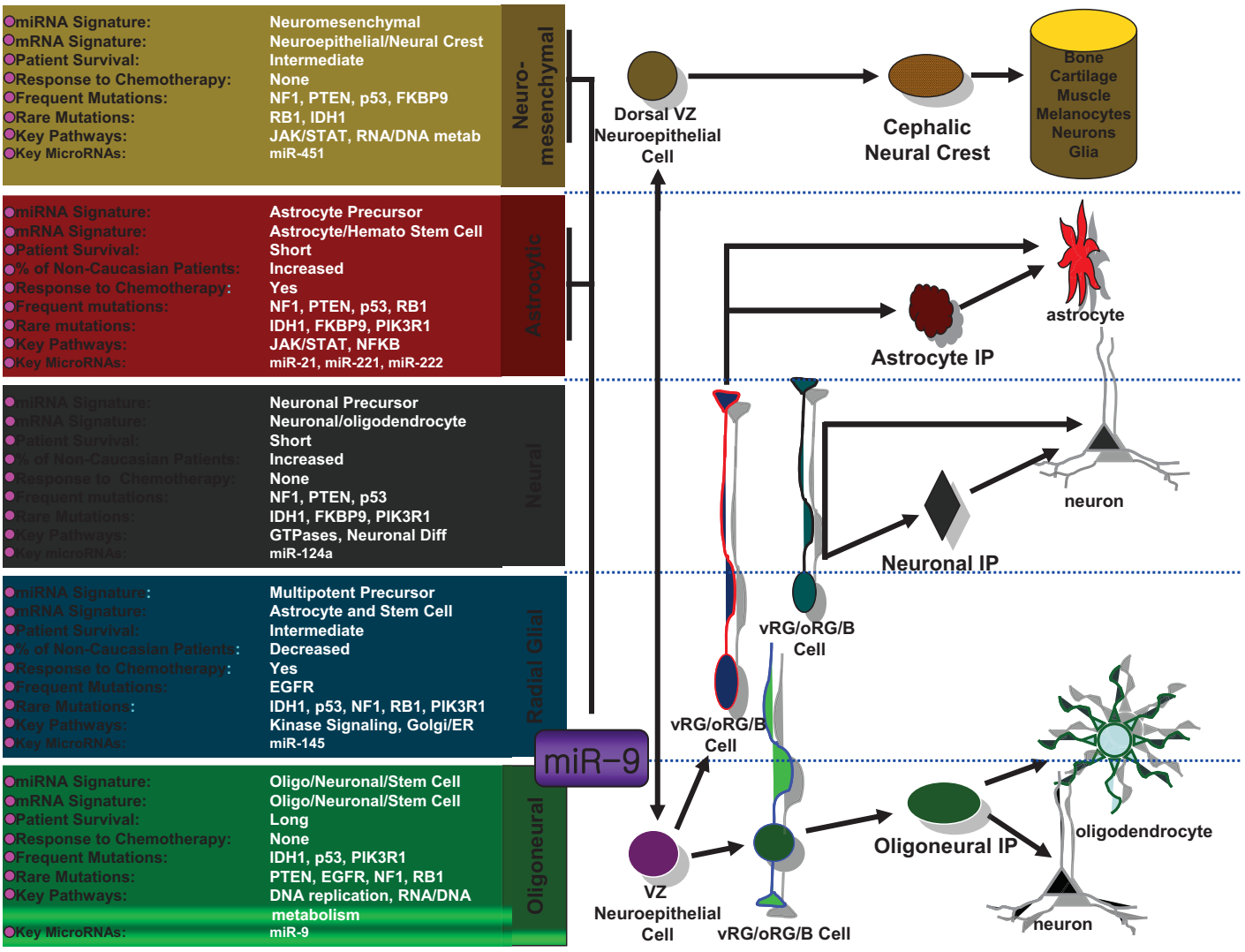

Figure S11. Summary diagram of microRNA-based glioblastoma classification. Schematic diagram summarizing the characteristics of five microRNA-based glioblastoma subclasses and their relationship to neural precursor differentiation. Characteristics of the oligoneural, radial glial, neural, neuromesenchymal and astrocytic glioblastoma subclasses are shown at left. Schematic diagram illustrating the corresponding stages of neural stem cell differentiation is shown on the right. The role of miR-9 in suppressing mesenchymal/astrocytic differentiation and maintaining the oligoneural and radial glial phenotype is also shown. VZ (ventricular zone); vRG (ventricular Radial Glial cell); oRG (outer Radial Glial cell); B (Type B cell); IP (intermediate progenitor).